ANNUAL REPORT

Wettability and Reaction Kinetics in Metal Matrix Composites

Submitted to:
Dr. Steven Fishman
Office of Naval Research
Arlington, Virginia 22217

Submitted by:
Glen R. Edwards and David L. Olson
Center for Welding and Joining Research
Colorado School of Mines
Golden, Colorado 80401

August 1993

This program supported by the Strategic Defense Initiative Office/Innovative Science and Technology under ONR contract N00014-92-J-1389.

CSM

CENTER FOR WELDING AND JOINING RESEARCH
Colorado School of Mines
Golden, Colorado 80401

TABLE OF CONTENTS

LIST OF FIGURES

1.0 Project Summary

Research accomplishments during the last academic year are in two related areas: a) further applications of the thermodynamic model developed in the previous years, and b) kinetic studies in alumina/reactive metal systems. The ongoing projects are adaptations of the research findings from the previous years, aimed at improving the wettability at an aluminum/alumina interface and understanding the nature of the oxide barrier formed at the ceramic/liquid aluminum interface.

1.1 Further Thermodynamic Predictions

A thermodynamic criterion was developed previously [1] to identify metals and alloys that are thermodynamically capable of wetting the ceramic surface. Wetting was assumed to be a surface phenomenon, and a surface reaction monolayer was considered sufficient to cause wetting. Using this approach a wettability map of magnesium oxide was prepared. The predictions were compared to actual experiments and to the contact angle measurements available in the literature [2].

To aid in the technological selection of appropriate metal-ceramic pairs, a unified wettability map for commercially significant oxide ceramics was developed. The oxide wettability diagram is simply a plot of the standard free energy of formation of both the bulk and surface phases of the ceramic. Also superimposed on the plot is the formation energy of the oxide of the reactive metal.

1.2 Kinetics Studies

Based on the thermodynamic studies, copper-titanium alloys were found to wet an alumina surface. Traditionally, other researchers have used contact angles as a measurable parameter to track the kinetics of wetting. For reactive wetting systems, the observed liquid drop morphology is perceived to be controlled by two independent phenomena - the reaction product formation beneath the liquid drop and the movement of the liquid drop ahead of the original triple point.

Kinetics of the initialstage were studied by monitoring the rate of interfacial phase formation. An immersion apparatus was used to study the initialkinetics independent of other phenomena associated with the later stages. The extent of reaction was measured both by surface compositional analysis and by interfacial reaction layer thickness measurements. The reaction layer exhibited a parabolic growth with an associated activation energy of 180-230 kJ/mole. A speculative growth mechanism was proposed based on the experimental observations and the information available in the literature.

1.3 Ongoing Projects

Titanium Preconditioning of Alumina

The solgas mix program has been successfully used to identify the appropriate activator for titanium chemical vapor deposition on alumina and graphite substrates. Preliminary experiments in quartz ampules produced coatings which were a few micrometers thick . An experimental apparatus is being constructed to produce these coatings on a more reliable basis. The effectiveness of the titanium precoating will

be evaluated using the currently functional immersion apparatus.

Characterization of the Oxide Barrier

An immersion apparatus was built to study the kinetics of reaction layer formation on various ceramics in contact with liquid aluminum. Reproducible results have been obtained using silica substrates. The progress of reaction is being monitered by measuring the mullite fraction formed on the substrate using the EDS spectrometer associated with the SEM.

2.0 List of Accomplishments

Journal Publications

1 "*Kinetics of Interlayer Formation in α-Al_2O_3/Copper-Titanium Alloy Interface*", PR. Chidambaram, G. R. Edwards and D. L. Olson -- submitted to **Met. Trans.**, 1993

2 "*Fundamental Approach to Micro-Designing Metal-Ceramic Composites*", PR. Chidambaram, G. R. Edwards and D. L. Olson, **Composite Interfaces**, vol. 1, No. 2, p. 127-140, 1993

Thesis

Chidambaram, P. R., "Thermodynamic and Kinetic Aspects of Reactive Metal Liquids in Contact with Oxide Ceramics", CSM Ph. D. Thesis No. 4319, Dec 1992

Published Abstracts

"*Wettability Predictions at Oxide-Ceramic/Metal Interfaces*", PR. Chidambaram -- Submitted to the American Council for consideration in the International Institute of Welding Granjon student competition. Also, presented at the American Welding Society Annual Meeting, Houston, TX, April, 1993

"*Fundamental Approach to Micro-Designing Metal-Ceramic Composites*", PR. Chidambaram, G. R. Edwards and D. L. Olson, -- Fourth Intl. Conf. on Composite Interfaces, Cleveland, OH, 1992

of the acid-treated sample, were recorded at low magnifications. For large reaction layers

3.0 Further Thermodynamic Predictions

3.1 *Introduction*

Wetting can be defined to occur when the liquid atoms establish atomic contact with the atoms on the surface of the solid. It was established earlier that a system can be considered wetting whenever a reaction layer forms at the interface. Using this principle in an earlier study resulted in a thermodynamic model to identify the metals that wet an aluminum oxide surface [1]. The model was used in the follow on study to predict wettability on magnesium oxide surfaces. Wetting was treated as a surface phenomenon, and a surface reaction monolayer is considered sufficient to cause wetting. A comprehensive oxide ceramic wettability map that identified the reaction wetting systems was also developed. The free energy of wetting for both the surface and bulk phases were plotted as a function of temperature.

The well-known Young equation can be written:

$$\gamma^{lv}\cos\theta = \gamma^{sv} - \gamma^{sl} \qquad (1)$$

where γ^{lv}, γ^{sv}, and γ^{sl} are the liquid-vapor, solid-vapor, and liquid-solid interfacial energies respectively. The $\gamma^{lv}\cos\theta$ term above is often taken as the wettability parameter. This value is a measure of the wettability, and was used in this study to compare theory with experiment. This approach is valid only for non-wetting systems. The theoretical predictions were verified using the experimental information available in the literature [2] for nonwetting systems. In wetting systems, the interfacial reaction results in an altogether new phase. A new interface is interposed between the metal and the ceramic,

and therefore the Young equation is no longer valid. The formation of a reaction layer was used as the evaluation criterion for wetting systems. Experiments were performed at Colorado School of Mines to investigate the formation of reaction layers in wetting systems.

3.2 Theory

According to the surface wetting model, the surface of magnesium oxide can be treated as a separate phase with unique associated thermodynamic quantities. A surface phase formation energy of the surface atoms, ΔG^{surf}, which is very similar to the bulk formation energy, ΔG°, can be defined. The atoms on the surface are at a higher energy than those of the bulk; and consequently, the formation energy of the surface atoms is less negative than the bulk formation energy. The energy of the surface phase, a value over and above the bulk value, can be represented in terms of Gibbs excess energy, G^{xs}:

$$\Delta G_{MgO}^{surf} = \Delta G_{MgO}^{o} + G^{xs} \qquad (2)$$

The procedure established to estimate G^{xs} involves the use of the experimentally estimated surface specific energy γ as indicated In Eqn. (3):

$$G^{xs} = \gamma A \qquad (3)$$

where A is the area attributed a mole of surface atoms. Standard procedures are available to calculate this area [3]. Surface specific energy at the temperature of interest can be calculated using Eqn. (4):

$$\gamma = \gamma^{o} - \Delta S^{s} \Delta T \qquad (4)$$

the depletion of titanium at the interface. Samples for the 0.5-w/o titanium alloy were

No standardized procedures exist for estimating the surface energy; however, a few published results are available. The surface specific energy at 0° K, γ^{o} and the surface specific entropy, S^{s}, used in the present study were 1300 mJ/M^2 and 0.22 mJ/M^{2}K respectively. The values were obtained from the study by Bruce [4]. Once ΔG^{surf} was calculated, the standard thermodynamic procedure can be used to evaluate the driving force for wetting in terms of the Gibbs free energy of wetting, ΔG_w. A reaction between the metal M of interest and the surface phase of MgO to form M_xO was written as:

$$xM + MgO^{surf} \rightarrow M_xO + Mg \tag{5}$$

The ΔG_w for this reaction is given by:

$$\Delta G_w = \Delta G_{M_xO} - \Delta G_{MgO}^{surf} + RT\ln\left[\frac{a_{Mg}}{a_M^x}\right] \tag{6}$$

The free energy of wetting is related to ΔG_r by Eqn (7):

$$\Delta G_w = \Delta G_r + G^{xs} \tag{7}$$

The activity of magnesium in the metal a_{Mg} was calculated by:

$$a_{Mg} = \Gamma_{Mg} X_{Mg} \tag{8}$$

Activitycoefficients, Γ, were obtained from the data book on thermodynamic properties of binary alloys [5]; if unavailable, an ideal behavior was assumed. The standard free energy of formation ΔG^{o} was readily available in the literature [6]. Calculations were performed for a temperature in excess of the melting temperature for the metal, and a

one percent dissolution of magnesium in the metal was assumed. The parameters used and the results obtained from the calculations are presented in Table 1.

3.3 Experimental Procedure

In non-reactive metal-ceramic couples, no new phase forms at the interface; therefore, the experimentally estimated contact angles will be consistent with the Young equation. The wettability parameters available in the literature for non reactive magnesium oxide-metal systems were used to verify the predictions. In the case of a reactive metal in contact with magnesium oxide, wettability was verified by confirming the formation of a reaction layer. Copper-30% Ti and Cu- 40% Mn alloys were melted on pure (99.9%), high density, magnesium oxide substrates (obtained from UBE industries Inc.) in a vacuum furnace. The alloys were prepared at an argon overpressure of 7 Mpa at 1250°C. The interfaces were investigated for reaction layers using the energy dispersive X-ray spectroscopy (EDS) attachment to the scanning electron microscope (SEM) and the X-ray diffractometer. Prior to X-ray analysis, the specimens were treated in 38% hydrochloric acid to dissolve the unreacted metal.

3.4 Results and Discussion

A positive ΔG_w was obtained for copper, iron, lead, nickel and lead, whereas a negative free energy of wetting was obtained for copper-titanium, copper-manganese and chromium. These observations are consistent with the experimental results obtained

interface can be identified. Figure 12e schematically illustrates the observed interface

in the present study, and with previously published results [2].

Copper-titanium and copper manganese alloys formed a reaction layer in contact with magnesium oxide. The copper-titanium alloy spread to 3 times the original drop size upon heating; however, the copper-manganese alloy spread only to 1.5 times the original size. Also, the copper-manganese alloy debonded from the substrate due to the thermal expansion mis-match.

Figure 1 shows the backscattered electron image of the copper-titanium alloy/magnesium oxide interface. Three distinct layers seen in cross-section are: magnesium oxide, a reaction layer, and a copper-titanium alloy (two phase microstructure). The X-ray line scan profiles revealed a titanium-rich interfacial layer, an observation which implies a chemical reaction between magnesium oxide and titanium.

The copper-manganese alloy could not be studied in cross section because the sample delaminated at the ceramic phase. Figure 2 shows the manganese and magnesium X-ray maps on the metal side of the interface. The manganese X-ray map appears complimentary to the magnesium map, suggesting that the delamination front traversed both the ceramic and the alloy. Such a delamination is possible only when interfacial bonding is significantly strong. The atom fraction of copper probed from the surface measured less than 2 percent. These observations indicate beyond doubt that Cu-40 % Mn alloys reacted with magnesium oxide. This is a striking verification of the model because the bulk thermodynamic calculations predict a large positive value for manganese reacting with magnesium oxide.

A wettability map (a plot of the predicted ΔG_w against the measured $\gamma^{lv}\cos\theta$) was

parabolic curve. Perhaps, the titanium content at the interface was depleted after 600

drawn to summarize the surface wetting model predictions (Figure 3). The wetting and non-wetting regimes shown in the plot correspond to a negative and positive free energy of wetting respectively. Non-reactive metals such as copper, tin, nickel, iron and lead fall within the non-wetting regime (region 6). Manganese, chromium and titanium and their respective alloys fallwithin the wetting region. As previously discussed, the $\gamma^{h}\cos\theta$ term is meaningless for wetting systems. Therefore, the data points in the wetting regime are shown as vertical lines corresponding to the appropriate ΔG_w values. The regions 3 and 4 are physically meaningless regimes; the absence of any data points in those regimes corroborates the model.

The uniqueness of this approach is its ability to accurately predict a wetting behavior for titanium, manganese and chromium (region 2). The wetting regime also encompasses a bulk reaction regime (region 1). A solid line is drawn where ΔG_r is zero. The difference between ΔG_r and ΔG_w is the surface excess energy G^{xs} (Eqn. 7), which is a function of temperature. A chemical reaction can occur at any point to the left of this line. (Note that ΔG_r predicts that a reaction between titanium, manganese or chromium and magnesium oxide is unfavorable).

Maps of this nature are useful in identifying the pairs that form stable interfaces. If a particular metal falls within region 1 of the map, reaction between the bulk phase of magnesia and the metal is limited only by the kinetics of the interface formation. With sufficient mass transport, a large interfacial reaction zone will be formed. The interfacial reaction products are typically brittle, and have a deleterious effect on many applications of the metal ceramic component. Titanium, manganese alloys, and chromium fallwithin

region 2, where the metal exhibits sufficient thermodynamic activity to reduce the surface of the ceramic but not the bulk. This situation results in a stable interface between the metal and the ceramic. The metal reduces the surface atoms of the ceramic; once the surface atoms are depleted, an equilibrium interface is formed. Such interfaces provide the required atomic contact without generating thick interfacial reaction layers. Therefore, metallic elements or alloys falling in region 2 of the map are ideally suited for composites processing for the ceramic substrate in question.

Oxide Wettability Diagram

To aid in the technological selection of appropriate metal-ceramic pairs, a unified wettability map for commercially significant oxide ceramics was developed. The free energy of reaction, ΔG_r, and the free energy of wetting, ΔG_w, are numerical sums of two independent energy changes: a) the energy released by the formation of the reactive metal oxide at the cost of the cation in the oxide ceramic lattice (difference in standard formation energy of the two oxides), and b) the energy released by dissolution of the displaced metal in the reactive alloy (the logarithmic terms in Eqn 6). More often than not, the latter energy is an order of magnitude less than the former. Ignoring the dissolution energy, a unified wettability map can be drawn. Similar to the Richardson diagram, this diagram is a plot of free energy change as a function of temperature (Figure 4). The standard free energies of formation for both the bulk phase, ΔG^{bulk} and the surface phase, ΔG^{surf} for alumina, magnesia, zirconia and silica are plotted. The details of the surface formation energy calculations for alumina and silica are published

elsewhere [1,7]. The ΔG^{surf} values were obtained by assuming that the ratio for the bulk to surface formation energy of zirconia was the same as that for alumina. Also shown superimposed on the plot are data points corresponding to the free energy of formation for the reactive oxide of each metallic alloy. The temperature for each reactive metal was chosen to be a value of 100°K above the melting point. Only the commonly utilized ceramic-metalic alloy compositions have been incorporated in Figure 4. The formation of surface and bulk phases of the ceramic are plotted as lines, while the formation of the reactive metal oxides are plotted as data points at the 100° K superheat temperature. (Of course, the formation energies for the reactive oxides also vary with temperature, but were plotted as points in Figure 4 to simplify the drawing).

Whenever the data point representing a given reactive metal oxide falls at a lower free energy value than the line for a particular ceramic phase, that particular liquid alloy will have sufficient thermodynamic potential to wet the ceramic phase. It was demonstrated earlier that an ideal matrix alloy (one which forms a stable interface with the ceramic) will lie in region 2 of the wettability map. An analogous requirement for the oxide wettability diagram implies that the liquid alloy should fall between the formation lines of the surface and bulk phases for the ceramic oxide. The commercial brazing alloys for ceramics such as Ticusil[1] are copper-silver-titanium based alloys. As can be seen from the diagram, these alloys fall between the bulk and surface formation lines of all commercial oxide ceramics, and hence, are ideal matrix alloys to be used with these ceramic reinforcements.

---

[1] Ticusil is a registered trade marked product of GTE

3.5 Conclusions

The surface phase thermodynamic criterion; i.e., that wetting occurs whenever ΔG_w is negative, was found to be true for magnesium oxide-metal interfaces. Also, the surface wetting model was found to predict accurately the metals or alloys which form stable interfaces with magnesium oxide. The oxide wettability diagram summarizes the wettability potential for common commercial oxide ceramics and the reactive metal alloys. The wettability maps and the oxide wettability diagrams have been shown to be successful in predicting appropriate metallic matrices for a given ceramic oxide reinforcement.

4.0 Kinetics Studies

4.1 Introduction

Many studies have measured contact angle to monitor the progress of wetting. Extensive time dependent contact angle information is available for the alumina-copper titanium alloy system [8,9]. Contact angle is related to the various interfacial interfacial energies according to Equation 1, and quantitative estimates of these energies are required to interpret the contact angle data. Reasonable estimates of the solid and liquid vapor surface energies are available in the literature; however, the solid-liquid interfacial energy is not directly measurable.

Theoretical procedures to quantitatively estimate the interfacial energies are available for metallic systems [10]; however, in metal-ceramic systems, there is little

agreement over the meaning of the interfacial energy term - particularly when wetting is accompanied by a reduction reaction. Chemically wetting systems rely on irreversible chemical bond formation at the interface; when new interfacial phases form, a new interface is interposed and the simple surface tension balance presented in Equation 1 is no longer valid.

Some studies [11-13] in the past have recognized this fact, and have adapted the Young equation to reactive wetting systems by incorporating the free energy change of the reaction into Equation 8. According to Aksay [11], most reactive wetting systems are thermodynamically in a non-equilibrium condition, where the reaction layer grows by mass transport across the interface. The mass transfer causes a gradual decrease in the interfacial energy, by an amount equal to the free energy change involved in forming the reaction product. Based on a similar analysis, Loeheman [12] developed a mathematical equation that relates the free energy change to the contact angle:

$$\gamma^{sv} - [\gamma^{sl} + \gamma^{ss}] + A\Delta G = \gamma^{lv}\cos\theta \qquad (9)$$

Laurent [13] used a slightly different approach to correct the contact angle:

$$\cos\theta = \cos\theta' - \frac{\Delta\sigma_r}{\gamma^{lv}} - \frac{\Delta F_r}{\gamma^{lv}} \qquad (10)$$

In this equation, $\Delta\sigma_r$ corrects for the interface created by the new phase formation, and ΔF_r incorporates the effect of the energy change from the reaction.

The Young equation is an equilibrium description of the surface tension balance at the interface; correcting this equation for the non-equilibrium reactive wetting systems seems questionable. It not clear that the energy released during the interlayer reaction

should influence the contact angle. Furthermore, the experimentally observed contact angle could be the manifestation of the incomplete coverage beneath the liquid drop. A small volume of liquid metal is extremely complicated to model when subjected to various forces such as the spreading force, the viscous drag force, and the gravitational force [14].

In the present analysis, contact angles and the associated wettability parameter were not used to evaluate chemically wetting systems. The dynamics of a reactive alloy drop spreading on a ceramic can be studied as two distinct phenomena, as shown in Figure 5. In Stage I, a reaction layer forms beneath the liquid drop, and in Stage II, the liquid drop spreads beyond the original triple point. The experimentally observed contact angle is the dynamic manifestation of these two concatenated events.

During Stage I (Figure 5b), the reactive metal in the liquid alloy is consumed both by the reaction with the ceramic and by oxidation on the surface of the liquid drop. An immersion experiment that isolates the reaction was developed to study the reaction rate independent of the oxidation.

In Stage II(Figure 5c), the movement of the liquid front ahead of the original triple point, often described as spreading, usually occurs after the liquid drop has attained a zero degree contact angle. In reactive wetting, this is not true; the liquid drop can assume an acute angle even when there is a driving force for spreading. The angle subtended by the drop is a manifestation of various kinetic events, and the angle can decrease only after the liquid drop has moved to an unreacted area. When the reactive alloy first comes in contact with the ceramic substrate, no reaction has occurred; hence,

the drop does not yet wet the ceramic surface. In this situation, the interfacial energy, γ_l^{sl}, is largely positive and can be calculated using the Young equation. The alloy then reacts with the ceramic according to Stage I kinetics and causes the liquid drop to assume an acute angle. The liquid drop experiences two distinct interfacial energies from the reacted and the unreacted fractions of the surface. This γ^{sl} is a function of coverage on the ceramic surface and therefore, is a function of time, temperature, and composition of the reactive component of the alloy. Understanding the kinetics of stage I was the main objective of this study.

4.2 Experimental Procedure

A simple experimental approach of immersing the aluminum oxide coupons into the pre-prepared molten alloy (maintained at the temperature of interest), and quantitatively characterizing the interlayer reaction product was developed to measure the wetting kinetics.

Homogeneous alloys of copper-titanium required for immersion experiments were prepared in an induction furnace. Each sample was melted in an evacuated and argon backfilled quartz chamber. A LEPEL high frequency generator was used to generate the field around the induction coil. A graphite foil sleeve prevented any reaction between the graphite crucible and the copper-titanium alloy.

Immersion experiments were performed in a sealed mullite chamber, which was evacuated using a mechanical pump and backfilled with high purity argon. The argon

gas was recirculated through the molecular sieve to scavenge the moisture in the chamber; the recirculation system was overpressured by seven kilopascals to prevent any air infiltration. The schematic diagram in Figure 6 illustrates the technique. The furnace was slowly raised to the test temperature and stabilized at this temperature for 1800 seconds. Known lengths of aluminum oxide (AD-996) strips (20 mm by 50 mm in dimensions) were cumulatively inserted into the molten alloy of interest for varying lengths of time. Copper-titanium alloys of various compositions (0.5, 1.0, 5-w/o titanium) were immersed, at three different temperatures (1100, 1150, 1180°C). The immersion times were varied between 60 to 1800 seconds for all the tests. The immersion times and compositions were chosen to study the reaction kinetics at the initiation of the reaction. The sample was then cooled in the furnace after the test at a relatively slow cooling rate.

The samples were characterized using the energy dispersive X-ray spectroscopy (EDS) attachment to the Scanning Electron Microscopy (SEM). A JEOL JXA840 SEM with a Tracor Northern EDS spectrometer was used for the purpose.

Two different techniques were required to adequately measure the reaction layer thickness. The reaction layer thickness was found to vary between 0.2 and 3.5 micrometers. Small layer thicknesses (1.0 and 0.5-w/o titanium samples), were analyzed by the surface EDS technique. After immersion, the unreacted metal was dissolved using 38 percent hydrochloric acid for 600 seconds. The surface was then probed by the EDS spectrometer. The ratio of the EDS fractions from the reaction layer and the substrate was a measure of the reaction layer thickness. EDS spectra from the surface

of the acid treated sample were recorded at low magnifications. For large reaction layers (5.0-w/o titanium samples), the surface EDS technique could not be used and the titanium reaction layer was measured from a backscattered electron SEM image of the interface. X-ray line scans were acquired from the polished interfaces to monitor the interlayer compositions. Prior to acid treating, a small section of the sample was cut and metallographically polished in cross section down to one micrometer using a diamond polishing wheel.

4.3 Results

Surface EDS Technique

The surface EDS technique was found to more accurately assess the reaction layer growth kinetics than the direct interface measurements. Each immersed ceramic strip contained five reaction zones (one for each exposure time). The various reaction zones were identified using the back-scattered electron image in the SEM. Figure 7 shows the micrograph contrasting the 600-s zone from the 300-s zone on the surface of alumina immersed in copper containing 1.0-w/o- titanium alloy at 1150°C. The unreacted metal, physically present on the specimen surface, was leached out using an acid solution prior to EDS analysis. No copper was detected in the EDS analysis, even though the alloys contained up to 99.5-w/o copper.

The X-ray sampling depth is approximately 1.5 micrometer for a titanium oxide

material. If the reaction layer is less than the sampling depth, the signal from the substrate is also registered in the detector. The ratio of the substrate peak to the reaction layer peak is a measure of the reaction layer thickness. Three sets of EDS data at low magnifications were collected from each zone. The relative percentages of titanium and aluminum were obtained from the EDS spectrum using the curve fitting software associated with the X-ray processor. From these sets of data, the mean and standard deviation of each composition were determined. The results of the statistical analysis are shown as (95 percent confidence limit) error bars in the plots (Figure 8-10).

Figure 8 is a plot of the EDS titanium and aluminum signals measured as a function of the immersion time for alumina immersed in copper 1-w/o titanium alloy at 1100°C. As discussed above, the aluminum and the titanium percentages correspond to the substrate and the reaction layer respectively. As the titanium content increased, the aluminum signal decreased. The increase in the titanium content was parabolic with time for times less than 600 seconds. The growth rate decreased considerably after 600 seconds. The plot (Figure 9) for the 1.0-w/o titanium samples at 1150°C was recorded at a 20-keV accelerating voltage. The sampling depth can be increased in the SEM by increasing the accelerating voltage. The results obtained for the case of the copper 0.5-w/o titanium alloys are shown in Figure 10. The reaction layer growth, measured as the increase in the titanium atom percent, was parabolic for times less than 600 seconds. The reaction terminated at the end of 600 seconds for 0.5-w/o titanium alloys, and the plots show a saturation of the titanium signal. The reaction layer thickness increased with an increase in temperature. The apparent decrease in the growth rate was attributed to

6.0 Reference

the depletion of titanium at the interface. Samples for the 0.5-w/o titanium alloy were immersed at 1125°C as opposed to 1100°C because the melting point of this alloy was close to 1100°C.

The interface specimens were prepared from these zones also. Even though the reaction layer could not be identified in the backscattered electron SEM micrograph, an X-ray line scan revealed the thickness of the titanium peak at the interface. The X-ray line scans obtained from the various samples are published elsewhere [15]. The EDS titanium content was later correlated to the reaction layer thickness using the X-ray composition profiles. EDS compositions could be acquired from all the reaction zones with relative ease. In contrast, thickness measurement from the interface microstructures and X-ray line-scans were very sensitive to the surface features and polishing artifacts at the interface. Therefore, meaningful profiles could not be obtained from many zones, particularly when the reaction layers were less than one micrometer thick. To convert the EDS titanium atom percent from the surface to the reaction layer thickness, the EDS reading and the X-ray line scan measurements were correlated for both 15- and 20-keV accelerating voltages (the results are shown in Figure 11). A linear correlation is drawn in the plot; however, the lines did not extrapolate to zero. The electron interaction with the specimens in a SEM results in a pear shaped penetration profile; consequently, the lateral spreading of the beam varies with the penetration depth. For the present study, the thicknesses were measured at values which occurred near the middle of the interaction volume, and a linear approximation was considered adequate.

Acta. Metall. Mater., Vol. 40, No. 6, (1992), pp. 1167

Interface Micrograph Method (5.0-w/o-Ti Alloys)

At high titanium concentrations (5.0-w/o titanium), the surface EDS technique could not be employed because the reaction layer was thicker than the X-raypenetration depth. The reaction layer thickness then was measured directly from the SEM interface micrograph. An X-ray line scan was used to further validate the results. Unlike the surface EDS technique, this method is not very representative of the entire reaction zone. The interface can be sectioned at only one plane in cross section, and unless polishing is carefully done, polishing artifacts can mask the information at the interface. Since alumina is a hard material, a smooth interface could not be obtained. Also, some copper smeared from the bulk to the interface, thereby masking the interfacial microstructure. A statistical analysis, similar to the estimation of 95 percent confidence limits in the EDS compositions, could not be performed here. Figure 12 shows the backscattered electron image of the copper 5.0-w/o titanium/alumina interface immersed at 1180°C for 180 (Figure 12a) and 1800 seconds (Figure 12c). The X-ray line scan profiles (Figure 12b and 12d for 180-s and 1800-s repectively are also shown juxtaposed. A distinct gray area, corresponding to the reaction layer, can be identified at the interface. (The contrast in the backscattered electron picture had to be enhanced to such an extent that alumina appears black in some photographs). The growth of the reaction layer was non-uniform. The curvature appeared to correspond to the initial surface roughness of the alumina substrates (3-μm surface finish). Surface features on the sample also developed a gray contrast in the backscattered image. From the X-ray line scans, two distinct zones in the

18) Kofstad, Per., Nonstoichiometry, Diffusion, and Electrical Conductivity in Binary

interface can be identified. Figure 12e schematically illustrates the observed interface morphology. The phase adjacent to aluminum oxide was an oxide of titanium and the phase next to the metal was comprised of oxygen, copper and titanium. The exact stoichiometry of the complex Cu-Ti-O phase could not be identified. This observation is consistent with the results of Kritsalis et. al [9]. It is also obvious from the line scans that no aluminum peaks appeared within the reaction layer. In fact, at the point where the titanium peak appeared, no other element peaks were observed, indicating that the initial titanium-rich reaction layer did not contain significant amounts of aluminum or copper. The Ti-Cu-O layer was dissolved during acid treating in the surface EDS technique. Therefore, the growth of the Ti-O layer thickness was used to study the kinetics. The data obtained for the 5.0-w/o titanium alloy experiments are tabulated in Table 2.

4.4 Discussion

Two different rate constants, k_s and k_t were calculated. The rate of increase in the EDS titanium content for 0.5 and 1.0-w/o titanium alloys was defined as k_s, and the rate of increase in the reaction layer thickness (Ti-O layer) was defined as k_t.

The growth of the reaction layer in the 0.5 and 1.0-w/o titanium alloys was found to be parabolic for times less than 600 seconds. Figures 13 and 14 show the reaction layer growth for 0.5 and 1.0-w/o titanium alloys respectively as a function of the square root of time. The square of the slope of the lines in these plots is the parabolic rate constant, k_s. The value k_s represents the rate of increase in EDS titanium concentration as a function of time. The data points at 1800 seconds do not always fall on the

Table I. Model Parameters and Wettability Predictions for an Magnesium oxide Surface*

parabolic curve. Perhaps, the titanium content at the interface was depleted after 600 seconds, and further reaction occurred at a relatively slow rate. For the case of the 0.5-w/o titanium alloy, the reaction terminated at 600 seconds. For the 1.0-w/o titanium alloy at 1150°C, the reaction slowed down but did not completely stop.

It can be observed from Figure 13 that the curves do not extrapolate to zero coverage at the start of the reaction. At 1125°C and 1150°C an incubation time of 4 seconds was observed. This incubation time was used in calculating the rate constant, according to the equation:

$$k_s = (a/o - Ti)^2(t - t_o) \qquad (11)$$

where t_o is the incubation time. For 1.0-w/o titanium alloys, the reaction proceeded from the time of immersion; no measurable incubation times were observed. The incubation time is inferred to be related to the time taken for titanium to reach the interface, and therefore, was absent at relatively high concentrations of titanium.

The rate constant, k_s, is based on the EDS titanium content. A more meaningful parameter would be k_t, a rate constant based on the reaction layer thickness. The two rate constants can be scaled using the plot in Figure 11. The EDS titanium percentages were converted to the corresponding reaction layer thicknesses graphically, using the plot in Figure 11. This type of scaling is approximate. However, useful information concerning the relationship of the thickness to the EDS titanium content can be obtained. Thickness of the layer increased only after the entire surface was covered; hence, the conversion of the EDS content to thickness at the initial stages could be erroneous.

Table 2 Thickness of the reaction layer for the 5.0 w/o Ti alloy

The rate constant for the 5.0-w/o titanium alloy, k_t, was directly calculated from Figure 15, which is a plot of the reaction layer thickness as a function of the square root of time. The linear nature of this graph indicates parabolic growth. In this case, however, the reaction did not stop at 600 seconds. At high titanium concentrations, titanium was not depleted at the interface after 600 seconds. The k_t values were calculated for all temperatures and compositions of the alloys. The rate constants were calculated assuming a planar reaction layer growth. The actual reaction layer growth was observed to be non-uniform; however, this effect was judged to be unimportant to the analysis.

The temperature dependence of the rate constant, k_t, can be estimated using an Arrhenius-type activation energy analysis.

$$k_t = k_o e^{-\frac{Q}{RT}} \tag{12}$$

where Q is the activation energy of the rate controlling phenomena. A plot of the logarithm of the rate constant as a function of inverse temperature in degree Kelvin can be used to calculate the activation energy. Figure 16 is such a plot; the slope of this plot indicates an activation energy between 184 and 222 kJ/mole.

The activation energy represents the thermal barrier which must be overcome before the reaction proceeds. When the reaction involves many independent sequential processes, the slowest of the various steps controls the rate of the reaction, and the activation energy corresponds to this slowest step. Titanium interstitial diffusion in rutile has been found to manifest an activation energy of 250 kJ/mole [16].

In this experimental study, it is reasonable to assume that the reaction layer

possessed transport properties similar to those of rutile. An additional assumption then, is that the diffusion of cations (Ti and Al) through the reaction layer controlled the growth rate. The activation energy obtained, 200 kJ/mole, compares very well with the activation energy reported by Tressler et al. [17] of 216 kJ/mole for growth of reaction layers on alumina in contact with solid titanium.

Thermodynamic Analysis

A detailed thermochemical analysis of the system was conducted to identify the reaction products that can be formed at the interface. At the reaction temperature, the liquid alloy is a single phase solution containing copper, titanium and oxygen. When the alumina coupon is immersed in the liquid, titanium segregates to the interface, and alumina dissolves as aluminum and oxygen into the alloy. Both oxygen and aluminum released in the process can either react with titanium or dissolve in the liquid copper. The free energy of formation of various oxides of titanium and the other relevant free energy changes are listed in Table 2. As shown by the free energy changes suggested in Table 2, the oxygen released from the dissolution of alumina is more likely to react with the titanium present at the interface than dissolve in liquid copper. The partial molar free energy of oxygen dissolution in copper is only -25 kJ/mole compared to -69 kJ/mole for aluminum dissolution in copper. Therefore, aluminum can be expected to go into solution in copper. Also, the liquid alloy is expected to contain more than 600 ppm of oxygen. The available oxygen at the interface reacts with titanium according to the overall reaction

shown below:

$$\frac{1}{3}Al_2O_3 + xTi_{(Cu)} \rightarrow Ti_xO + \frac{2}{3}Al_{(Cu)} \qquad (13)$$

The 'x' in the above reaction determines the kind of titanium oxide which forms. Using the standard free energy of formation of the oxides and the partial molar free energy at infinite dilution, the above reaction would proceed in the forward direction for $x > 0.66$. This approach is relevant to the present discussion since titanium and aluminum are present at low concentrations in copper.

Interface Evolution

TiO and Ti(O) with a saturation composition of Ti_2O are the thermodynamically possible phases present at the interface. Once the reaction layer forms, the alumina substrate is covered rapidly. The results presented in the earlier section indicate that the reaction layer starts to grow at times much earlier than 60 seconds of immersion. The thickness of this layer increases with increasing time, temperature and titanium concentration in the alloy. The growth of the reaction layer is controlled by the diffusion of various species across the interface. Kritsalis et. al [9] modeled this interface as alumina in equilibrium with the liquid copper-titanium alloy. In the present study, a slightly different approach was adopted. The interfacial reaction occurring is described as a displacement reaction as shown in Equation 13. Figure 12e schematically illustrates the interfacial structure. It was shown earlier that TiO and Ti_2O were the oxide phases

that form at the interface. The growth of the interfacial layer stipulates that titanium ions diffuse from the liquid toward alumina, and that aluminum and oxygen ions diffuse in the opposite direction. The activity gradient of titanium and oxygen require that TiO form next to the alumina and that Ti_2O form adjacent to the copper-titanium alloy.

Even though the diagram shows distinct interfaces, the actual morphology is expected to be diffuse; thus, the stoichiometry should continuously change at the interface. Furthermore, the TiO lattice is known to be defect rich. Up to 35 percent of the lattice sites could be lattice defects, depending on the oxygen partial pressure [18].

The system under investigation can be considered as a diffusion couple between aluminum oxide and the copper-titanium alloy. Ideally, the estimation of the virtual diffusion path of the couple in the Al-Ti-Cu-O quaternary phase diagram would provide the fundamental insight into the reaction products formed at the interface. However, such a phase diagram was not available. An isothermal section at 1100°C of the ternary Al-Ti-O phase diagram was available from recent studies [19] (Figure 17). The diffusion paths obtained from Al_2O_3/Ti couple by Li et. al. are shown superimposed on the plot. Based on the work of Li [19] and Zang et. al [20] the interfacial layer sequence in an Al_2O_3/Ti diffusion couple was identified to be Al_2O_3/TiAl/Ti_3Al/α/β-Ti. No oxides of titanium were present in the pure titanium/alumina diffusion couples. In contrast, in the present study the interfacial reaction layer primarily consisted of oxides of titanium, and tianium aluminide intermetallics were absent. These observations are consistent with those of Kristsalis [9], who observed a similar microstructure. As mentioned before, when titanium is present at low concentrations as a solute in copper the thermochemistry is

significantly altered. Aluminum displaced from the oxide would dissolve more readily in the copper-rich liquid than oxygen. Therefore, the interfacial reaction product primarily contained oxides of titanium.

4.5 Conclusions

The contact angle can be argued to be a misleading parameter to describe the interfacial properties in reactive metal-ceramic systems. The rate of interfacial phase formation and the spreading kinetics both are consistent, alternate parameters to describe the kinetics involved in reactive metal-ceramic interfaces.

A successful experimental approach was developed to monitor the progress of reaction in alumina/copper alloy systems. The interfacial layer growth in the alumina/copper-titanium system was found to be diffusion controlled. An activation energy of approximately 200 kJ/mole was estimated from the experimentally measured rate constants. Cation diffusion through the reaction layer was speculated to be the rate controlling step in the growth phenomenon. The reaction layer was primarily an oxide of titanium. Ternary phase equilibria and solution thermodynamic principles were then used to explain the observed interfacial reaction product at the titanium-copper/alumina interface.

5.0 Experiments in Progress

5.1 Titanium Preconditioning of Alumina

It has been established that chemical bond formation with an associated electronic structure change at the interface is essential to generate a high bond energy interface between the metal and the ceramic [21]. In the Al_2O_3-Alsystem, such an interface formation is thermodynamically feasible. Unfortunately, this behavior is not experimentally observed [21].

Aluminum-oxide reinforced aluminum matrix composites have been difficult to produce by the inexpensive liquid processing route, due to incomplete interface formation between the liquid aluminum and the alumina substrate [21]. The inadequate wetting behavior can be attributed primarily to a low driving force for the reaction between aluminum and the aluminum oxide.

Titanium is known to react with the surface of the aluminum oxide and generate an aluminum-rich and titanium-rich interfacial reaction product [19]. The driving force for wetting is sufficiently large to develop complete coverage of the aluminum oxide surface [21]. As mentioned before, titanium supports multiple oxidation states. The inherent defect structure of titanium oxides allows the interface to tolerate large degrees of non-stoichiometry [21]. Due the tolerance for non-stoichiometry of the oxide layer, favorable composition and stress gradients could be obtained at the interface.

Chemical vapor deposition (CVD)was chosen to be the appropriate method to precondition the alumina substrate with titanium. Acommonly employed CVDmethod

is also known as pack cementation. This process involves heating the substrate to be coated in a pack containing titanium and a halide activator salt [22]. Titanium reacts with the activator salt to form titanium-halide, vapors which diffuse through the interstices of the aluminum oxide and deposit on the surface as metallic titanium. For this study HCl and NaCl were analyzed as possible transport species. These compounds react with titanium to form chloride vapors of titanium, such as: $TiCl_2$, $TiCl_3$, and $TiCl_4$.

To optimize the deposition environment, the public domain computer program 'SOLGASMIXwas used to estimate the thermodynamic activity of the various gaseous species at temperatures ranging from 1000K to 1700K. This program determines the partial pressures of various gaseous species by Gibb's free energy minimization approach. Chemical vapor deposition by the chosen activator is feasible when the partial pressures of the titanium-containing transport species are both one order of magnitude greater than that of the other reactive species, and greater than 10^{-5} atmospheres. Figure 18 is a plot of the partial pressure-temperature relationship for the most prominent gas species in the HCl activated environment.

Preliminary Results:

A feasibility study was conducted by depositing titanium in quartz ampules using NaCl and HCl as the activator species. The substrates were placed in the ampules along with the activator salt or gas, and titanium powder. The titanium-to-chloride molar ratio was maintained at 100:1. The ampules were evacuated and backfilled with argon and HCl gas prior to deposition. Depositions were performed between 700 and 1000°C.

The sodium chloride-activated chemical vapor deposition system did not produce adherent coatings on the alumina substrates. Allof the quartz ampules containing NaCl salt ruptured before reaching the deposition temperature.

The hydrogen chloride-activated chemical vapor deposition process produced a adherent titanium-rich layer on the surface of the alumina substrate. The layer thickness was on the order of a few micrometers.

Figure 19 is a backscattered electron image of the interface region. Energy dispersive spectroscopic (EDS) analysis showed the darker layer at the interface to be titanium rich. Atomic number contrast in backscatter electron imaging dictates that areas rich in higher atomic number elements appear brighter than areas rich in lower atomic number elements. The titanium-rich area of the interface should appear brighter than the aluminum rich substrate. However, this layer may appear darker because of interfacial erosion introduced during the polishing.

A more reliable CVD apparatus, designed with an on-line HCl gas train, is currently being constructed. The coating process will be characterized by a detailed time-temperature study.

The appropriate conditions determined from the above tests will be used to precoat the alumina substrates for immersion studies. The currently operational immersion apparatus will be used to evaluate the effectiveness of the preconditioning process in rendering the alumina substrate more wettable by molten aluminum.

5.2 Oxide Barrier Studies

The effect of the oxide barrier on composites processing with liquid aluminum is being investigated by immersion studies. The rate controlling step for the progress of reaction between aluminum and various ceramics substrates such as silica, graphite, and carbon is being measured. Since the oxide barrier formation is inherently related to liquid aluminum, the observed activation for progress of reaction is expected to be similar for all the substrates.

An immersion apparatus was built to immerse various substrates into liquid aluminum. A molten salt layer was maintained on the liquid aluminum surface to prevent the oxide layer from sticking onto the reacted surface and thereby masking the relevant extent of reactivity information. A ventilation system was constructed to exhaust the salt fumes. The progress of reaction will be monitored by the EDS analysis in the SEM, adopting a procedure similar to the analysis of reaction on alumina surfaces by titanium.

6.0 Reference

1) Chidambaram, P R., Edwards, G. R., and Olson, D. L., "A Thermodynamic Criterion to Predict Wettability at Metal-Alumina Interfaces", Met Trans Vol. 23 B, (1992 a), pp. 215

2) G. V. Samsonov, *The Oxide Handbook*, transl. by R. K. Johnston, (1982), Plenum Press, New York, pp. 400-408

3) K. S. Yeum, R. Speiser, and D. R. Poirier, Met. Trans. B, vol. 20, (1989), p. 693

4) R. H. Bruce, in *Science of Ceramics*, vol. 2, G. H. Stewart, editor, Academic Press, London, (1965), pp. 359

5) R. Hultgren, P. D. Desai, D. T. Hawkins, M. Gleiser: *Selected Values of Thermodynamic Properties of Binary Alloys*, ASM, Metals Park, Oh. USA, (1973), pp. 125-804

6) JANAF*Thermochemical Tables*, 2nd edition, U. S. Dept. of Commerce, (1977), p. 20-257

7) PR. Chidambaram, and G. R. Edwards, D. L. Olson -- Conf. Proc. Symposium on **Joining of Materials for 21st Century** in Trichirappalli, India, p. 331-338, Dec 1991

8) Naidich, Yu, "Wettability of Solids by Liquid Metals", Prog. in Surf. and Membrane Sci., Vol. 14 (1981), pp. 353

9) Kritsalis, P., Merlin, V., Coudurier, L., and Eustathopoulos, N., "Effect of Cr on Interfacial Interaction and Wetting Mechanism in Ni Alloy/Alumina Systems",

Acta. Metall. Mater., Vol. 40, No. 6, (1992), pp. 1167

10) Eustathopoulos, N., "Energetics of Solid/Liquid Interfaces of Metals and Alloys", Intl. Metl. Rews., Vol. 28, (1984) pp. 189

11) Aksay, I. A., Hoge, C. E., and Pask, J. A., "Wetting Under Chemical Equilibrium and Non-equilibrium Conditions", J. Phys. Chem., Vol. 78, No. 12, (1974), pp. 1178

12) Loehman, R. E., Tomsi, A. P., Pask, J. A., and Johnson, S. M., "Bonding Mechanisms in Silicon Nitride Brazing", J. Am. Ceram. Soc., Vol. 73, No. 3, (1990), pp. 552

13) Laurent, V., Chatain, D., and Eustathopoulos, N., "Wettabiliityof Monocrystalline Alumina by Aluminium Between its Melting Melting Point and 1273 K", Acta. Matall., Vol. 36, (1988), pp. 1797

14) Yin, T. P., "The Kinetics of Spreading", J. Phys. Chem. Vol. 7, (1969), pp. 2413

15) Chidambaram, P. R., "Thermodynamic and Kinetic Aspects of Reactive Metal Liquids in Contact with Oxide Ceramics", CSM Ph. D. Thesis No. 4319, Dec 1992

16) Sasaki, J., Peterson, N. L., and Hoshino, K., "Tracer Impurity Diffusion in Single-Crystal Rutile",J. Phys. Chem. Solids, Vol. 46, No. 11, (1985), pp. 1267

17) Tressler, R. E., Moore, T. L., and Crane, R. L., "Reactivity and Interface Characteristics of Titanium-AluminaComposites", J. Mater. Sci, Vol. 8, pp. 151, (1973)

18) Kofstad, Per., Nonstoichiometry, Diffusion, and Electrical Conductivity in Binary Metal Oxides, Wiley Interscience, New York, (1972)

19) Li, X. L., Hillel, R., Teyssandier, F., Choi, S. K., and Van Loo, F. J. J., "Reactions and phase relations in the Ti-Al-Osystem" Acta. Metall. Mater., Vol. 40, N0. 11, (1992), pp. 3149

20) Zhang, M. X., Hsieh, DeKock J., and Chang, Y. A., "Phase Diagram of Ti-Al-O at 1100°C, Scripta Metall. Mater., Vol. 27, (1992), pp. 1361-1366

21) G. R. Edwards, Research Proposal #3899, Colorado School of Mines, December 1992.

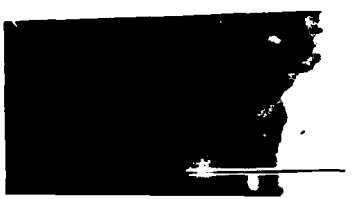

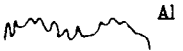

Table I. Model Parameters and Wettability Predictions for an Magnesium oxide Surface#

Metal Alloy	T °K	ΔG° kJ/mole	Γ_{Mg}	γ^{h} mJ/m^{2}	ΔG_{ad} kJ/mole	$\gamma^{h}\cos\theta$ mJ/m^{2} (ref)
Cu	1450	-28.1	0.15	1300	146.59	-1268 (8)
Ni	1826	-76.5	1	1660	42.48	-1191 (8)
Fe	1909	-142.3	1	1840	6.36	-867 (8)
Sn	605	-227.5	0.019	542	62.79	-1018 (8)
Pb	700	-148.7	0.01	442	101.26	-480 (8)
Cu-30%Ti	1450	-290	0.01	1300	-143.62	-
Cr	2225	-630.1	1	1590	-144.41	-
Cu-40%Mn	1615	-268.3	1	1060	-100.1	-

- calculations were performed for a 100 degree over the melting temperature.

Table 2 Thickness of the reaction layer for the 5.0 w/o Ti alloy

time (s)	$(time)^{0.5}$ $(s)^{0.5}$	thickness (μm) 1100°C	1150°C	1180°C
60	7.45			0.6
180	13.416	0.6	0.8	0.9
300	17.320	0.8	1.2	
600	24.494	1.0	1.6	2.0
1800	42.426	1.9	3.0	3.8

Table 3 The relevant free energy changes at 1100°C for Ti-Al-Osystem

Phase	ΔG kJ/mole	Reference
1/3 Al_2O_3	-410.264	JANAF77
$Ti_2O(\alpha Ti(O))$	-456.00	Li 92
TiO	-412.216	JANAF77
Ti_2O_3	-384.874	JANAF77
Ti_3O_5	-373.712	JANAF77
Ti_4O_7	-364.04	Li 92
TiO_2	-347.991	JANAF77
Ti_3Al	-18.377	Li 92
TiAl	-26.165	Li 92
Partial Molar Free Energy at Infinite Dilution ΔG_2		
$O_{\_Cu}$	-22.504	Murray 83
$Al_{\_Cu}$	-69.2	Hultgren
$Ti_{\_Cu}$	-24.28	Hultgren

Table 4 The free energy changes at 1100°C for the displacement reactions resulting in the formation of various titanium oxides

Phase	x	ΔG kJ/mole
$Ti_2O(\alpha Ti(O))$	2	-67.869
TiO	1	-24.085
Ti_2O_3	0.66	3.25
Ti_3O_5	0.6	14.418
Ti_4O_7	0.57	24.07
TiO_2	0.5	40.139

Figure 1 The back scattered electron image of the copper-titanium/magnesium oxide interface

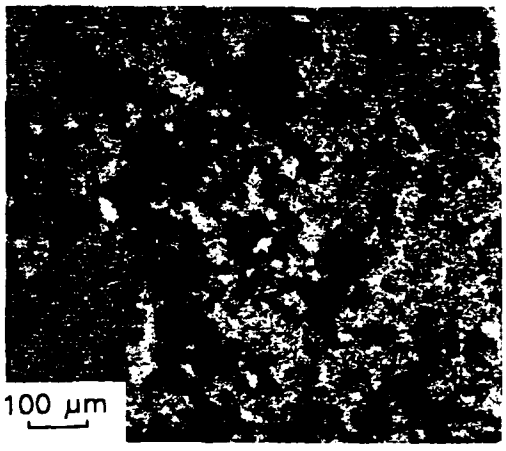

Figure 2 X-ray maps of the delaminated interface in magnesium oxide/copper-manganese alloy interfaces a) Manganese b) Magnesium

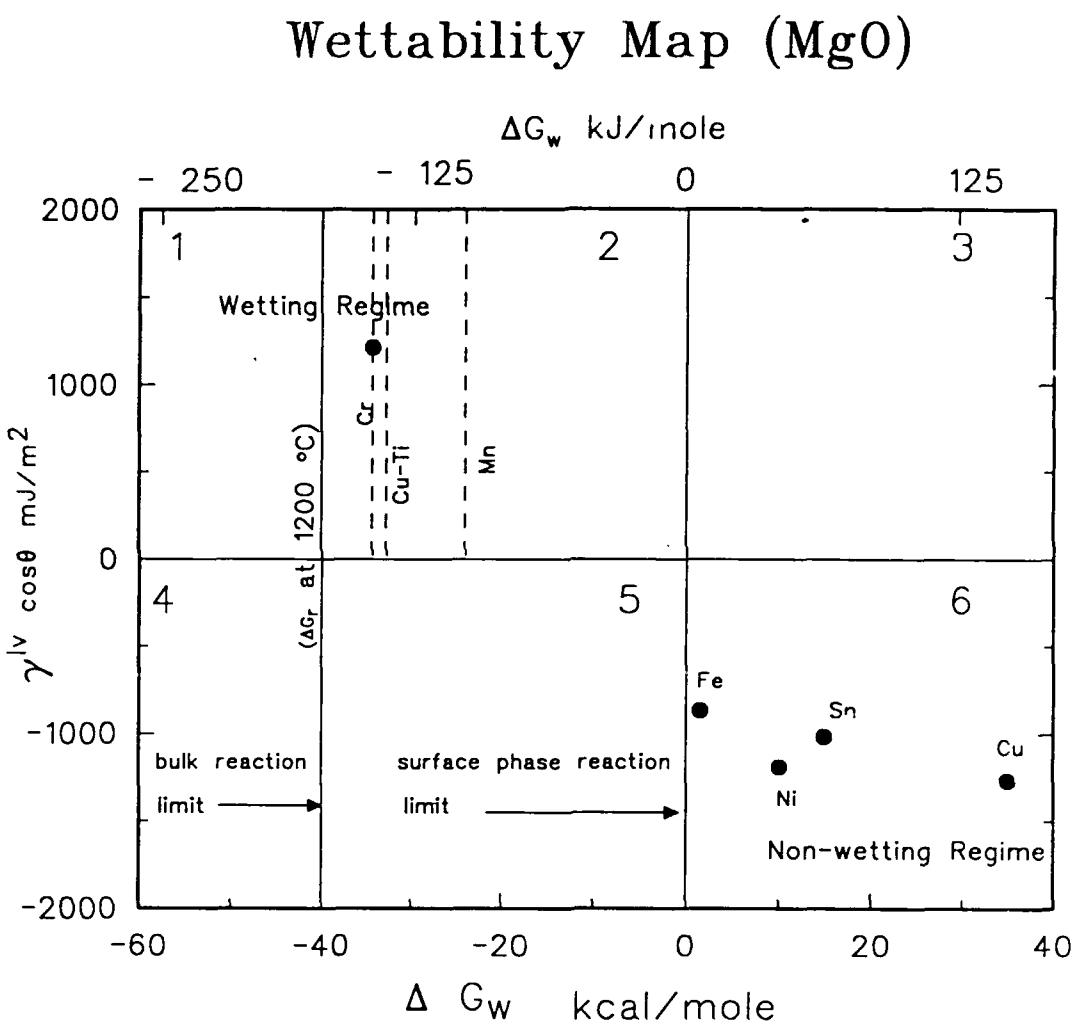

Figure 3 Wettability map for MgO. Temperature was chosen to be 100 degrees Kelvin above the melting point of the metal

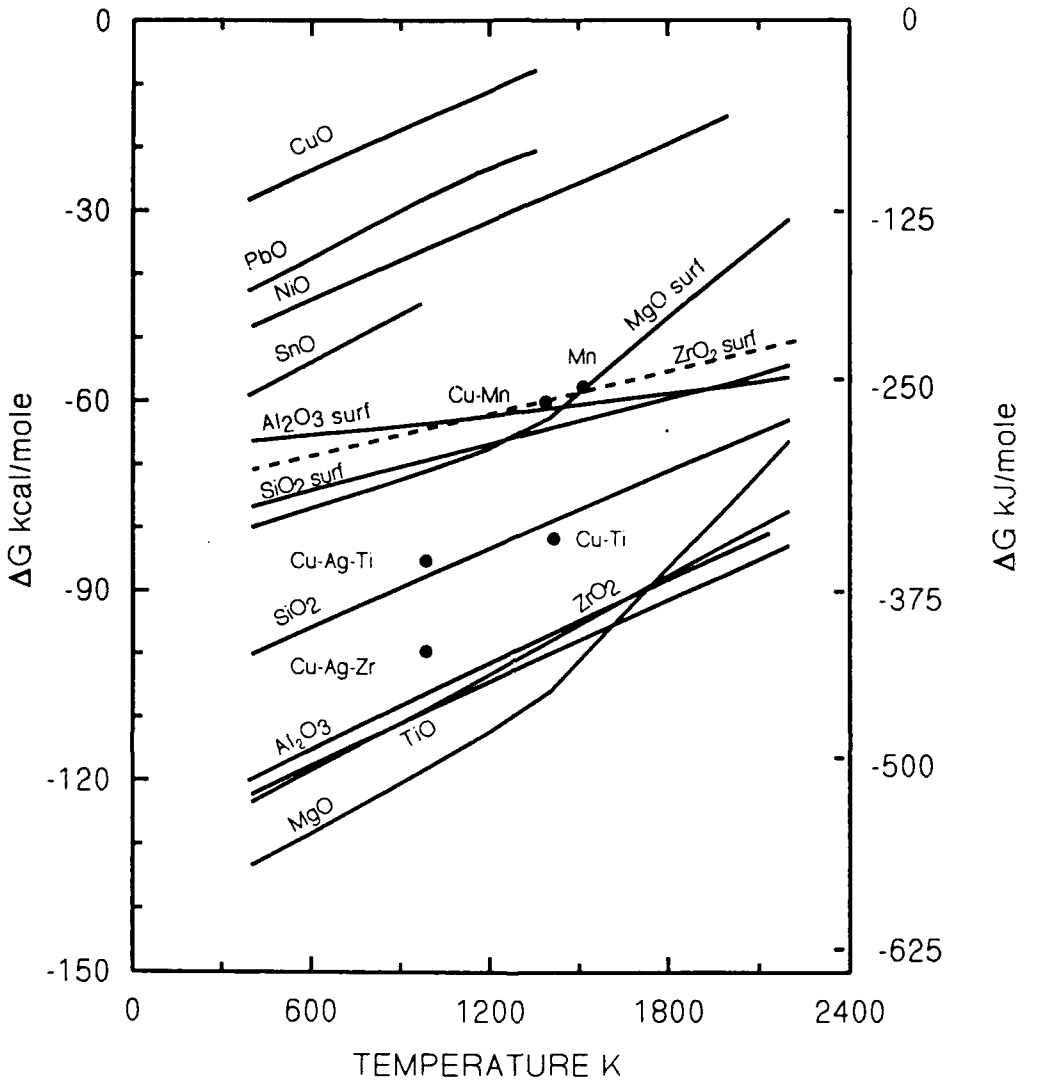

Figure 4 The oxide wettability diagram showing the reactivity of both the ceramics and the matrix alloys.

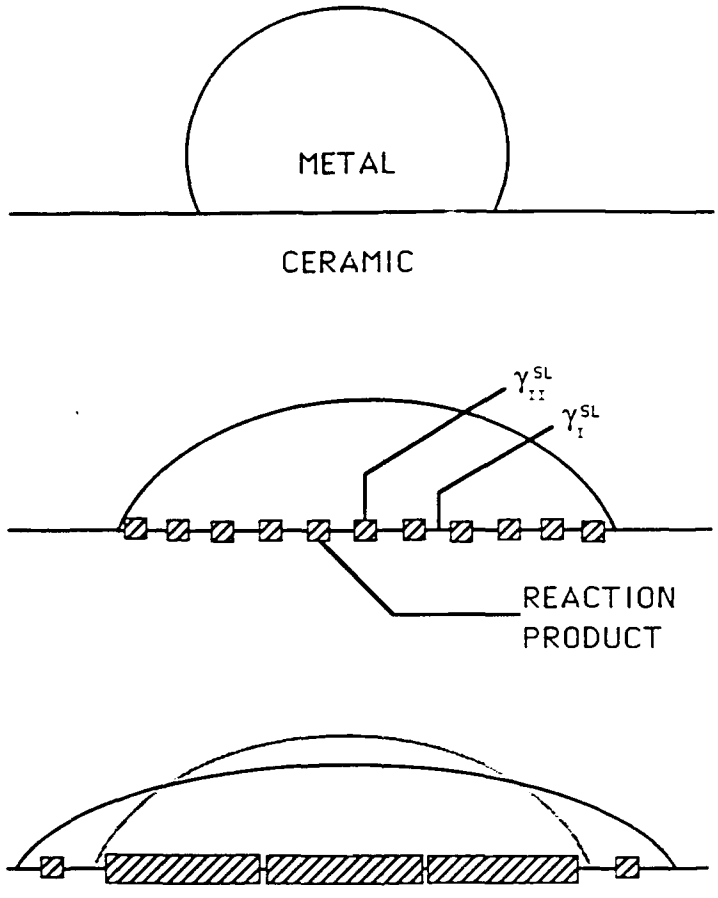

Figure 5 Schematic diagram illustrating the two stages involved in the spreading of a liquid drop

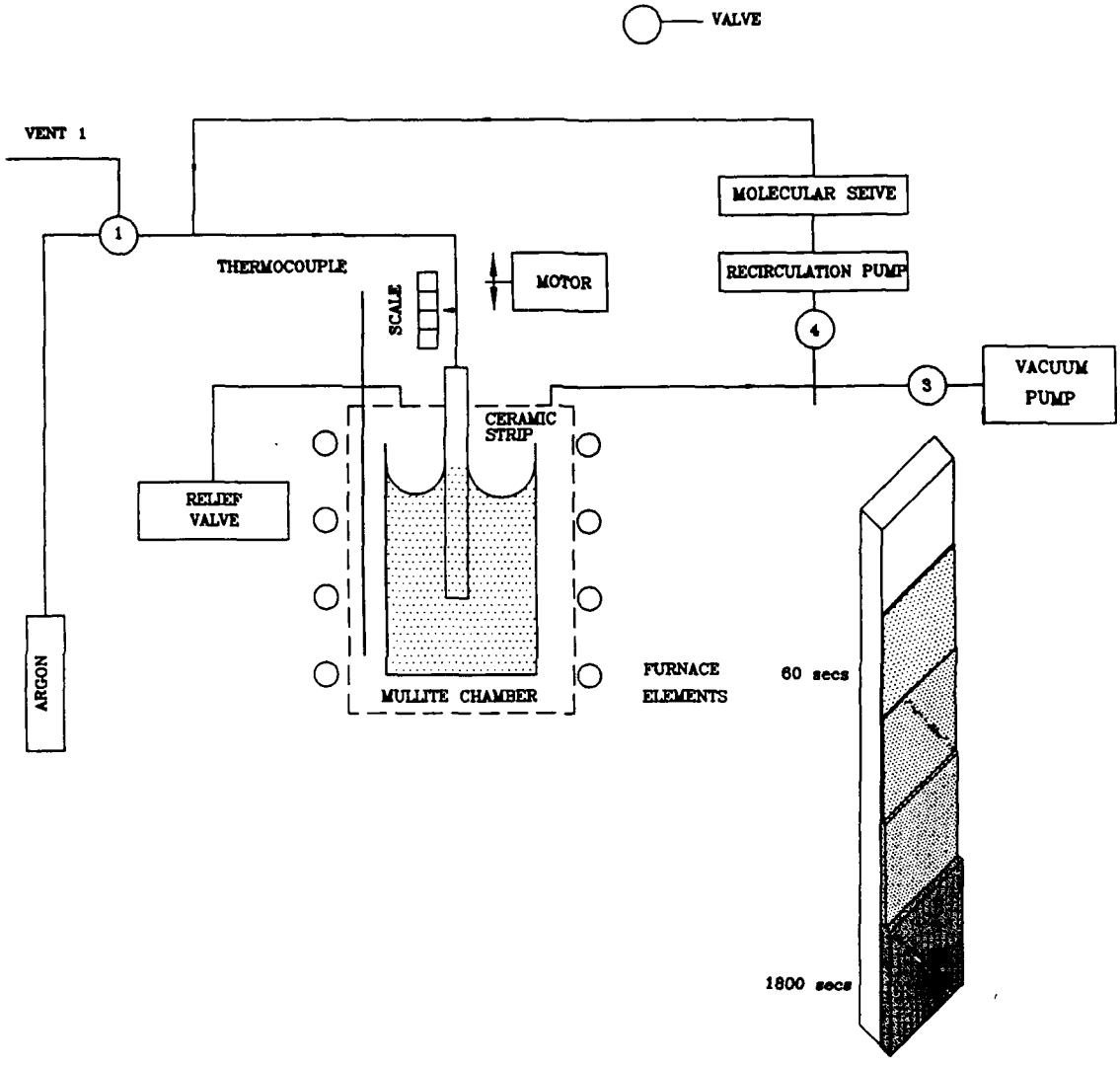

Figure 6 Schematic diagram of the apparatus used for measuring wetting kinetics

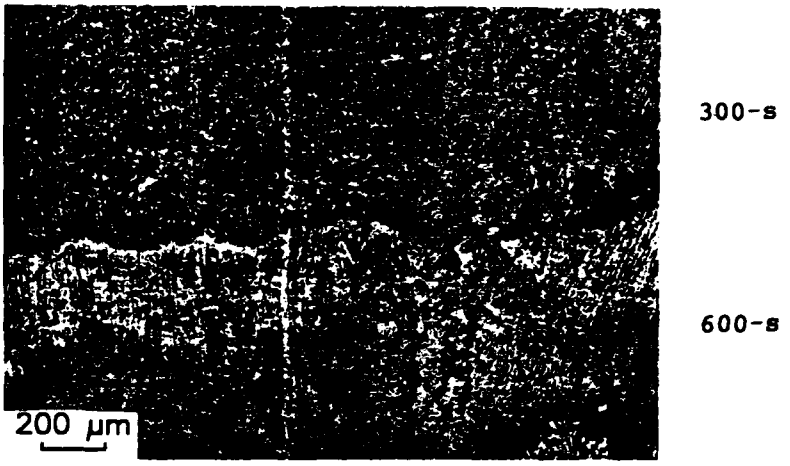

Figure 7 SEM backscattered electron micrograph contrasting the reaction zones on alumina after 600- and 300-s exposure in liquid Cu-1-w/o titanium alloy at 1150°C

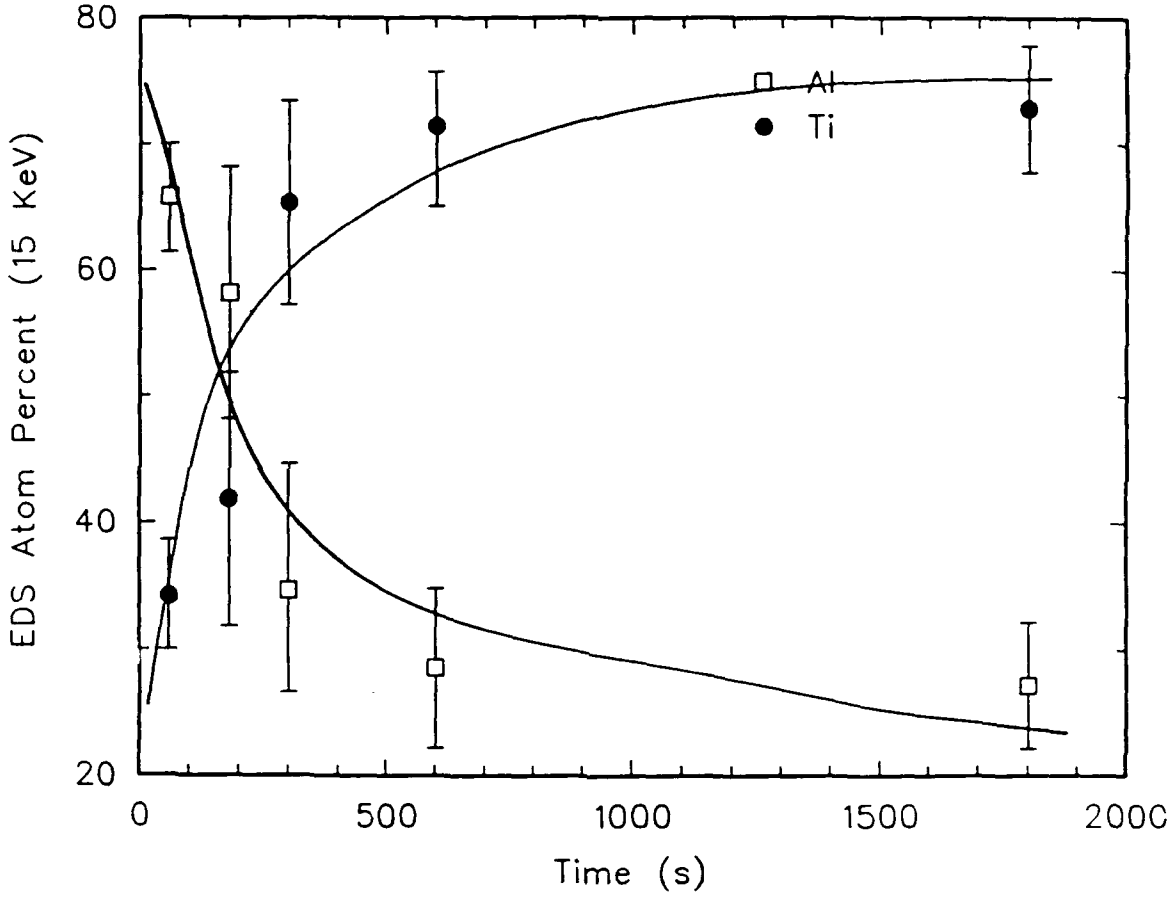

Figure 8 EDS spectrum (15-keV) from alumina substrate immersed in Cu-1.0-w/o-Ti alloy at 1150°C

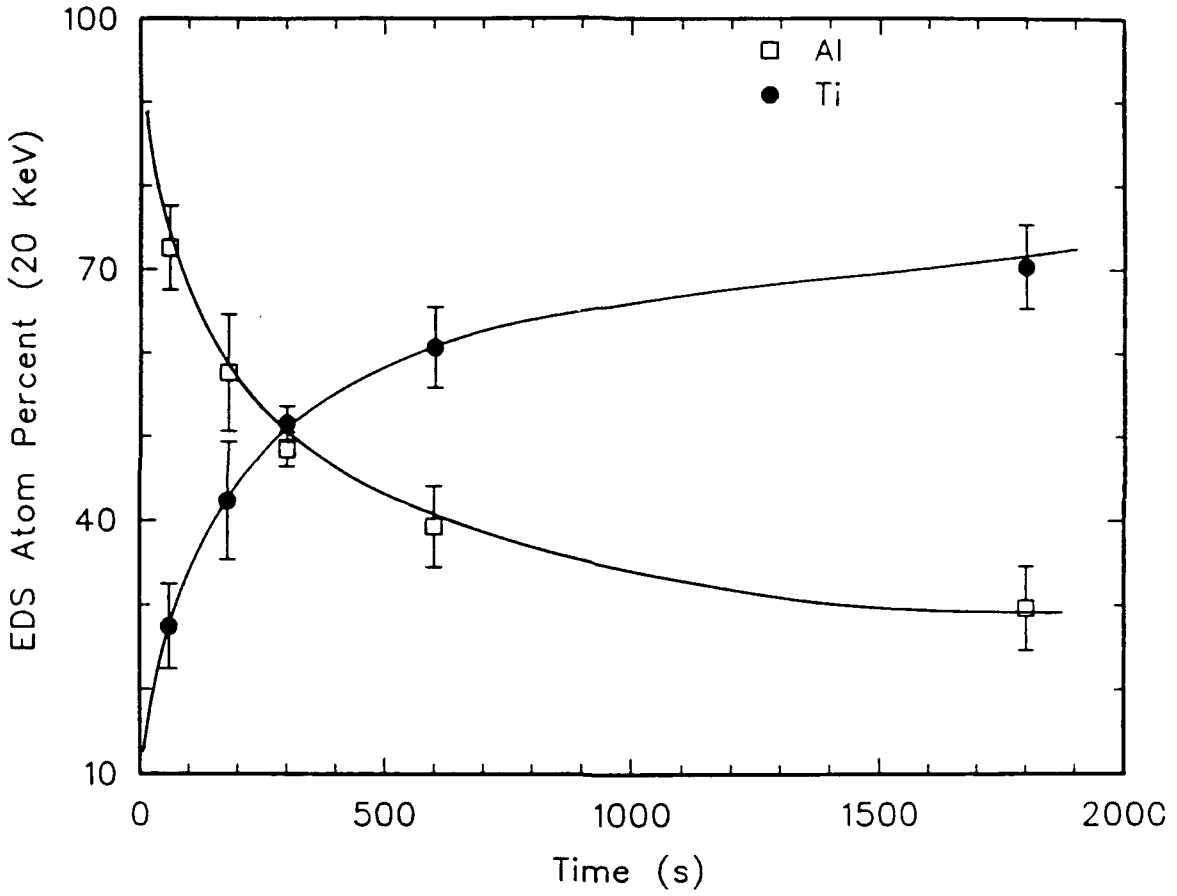

Figure 9 EDS spectrum (20-keV)from alumina substrate immersed in Cu-1.0-w/o-Ti alloy at 1150°C

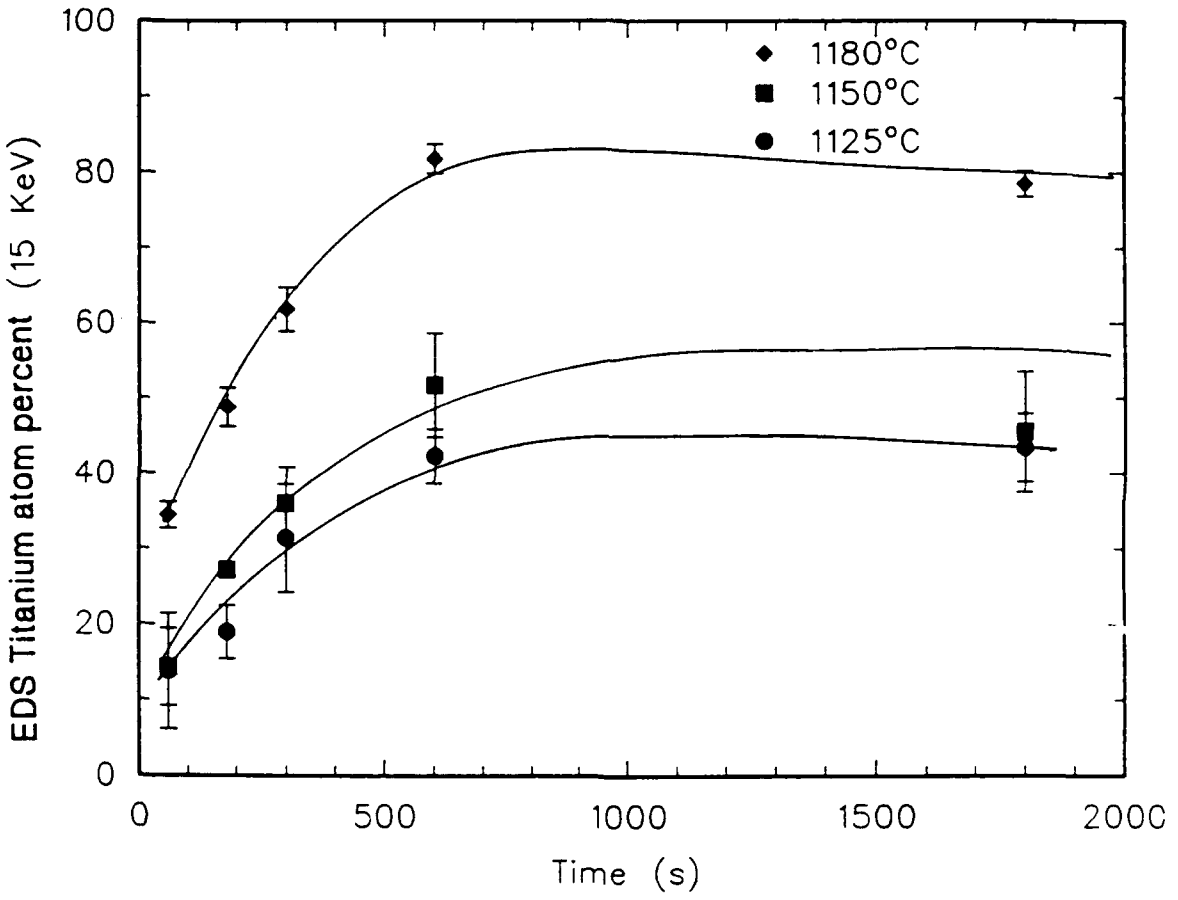

Figure 10 EDS spectrum (15-keV) from alumina substrate immersed in Cu-0.5-w/o-Ti alloy at 1125°, 1150° and 1180°C

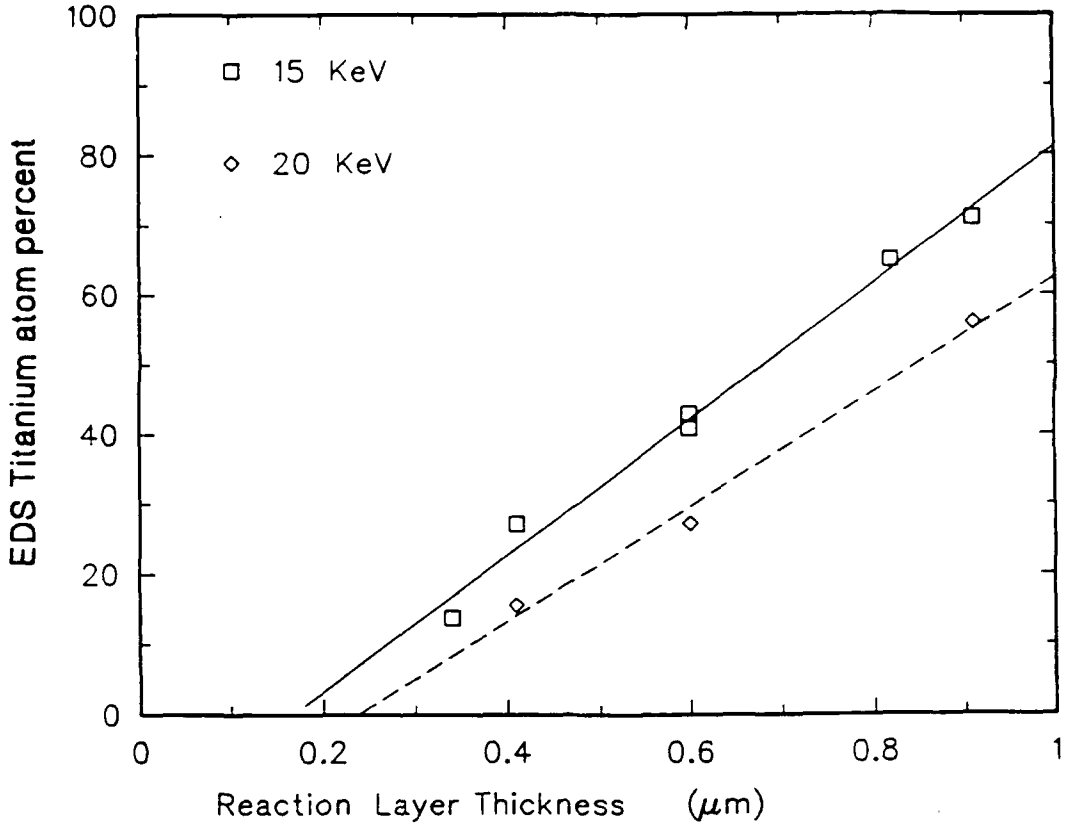

Figure 11 The correlation plot between the thickness of the reaction layer and the surface EDS titanium a/o

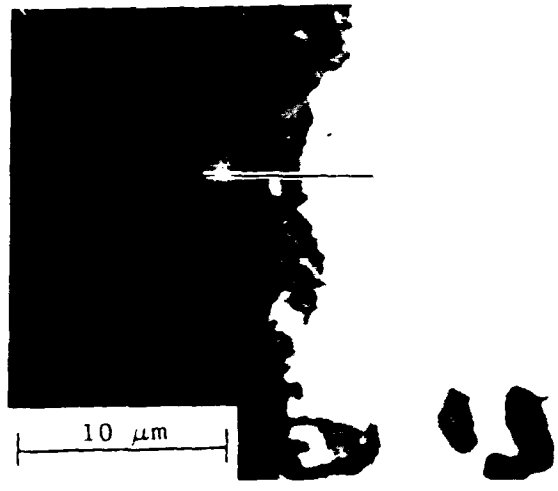

a

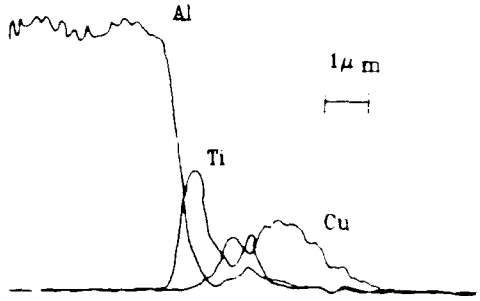

b

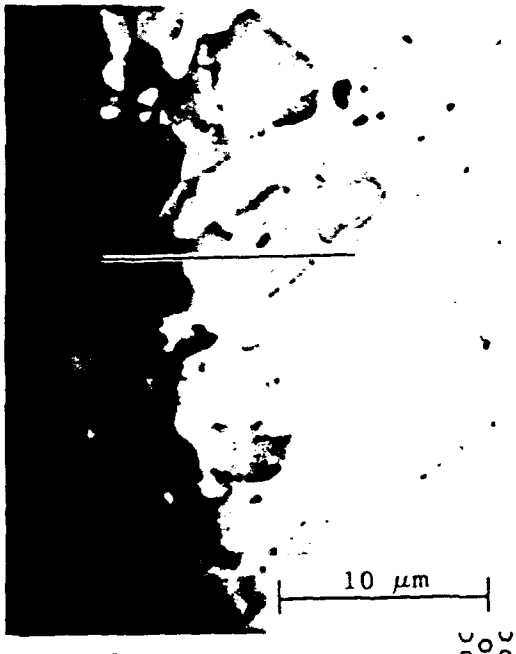

c

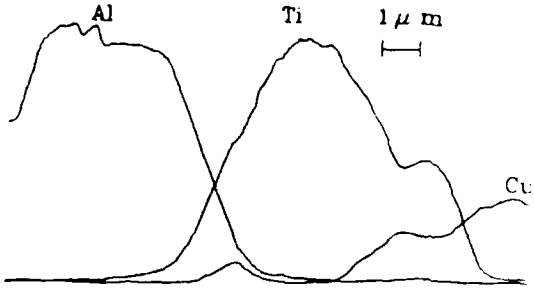

d

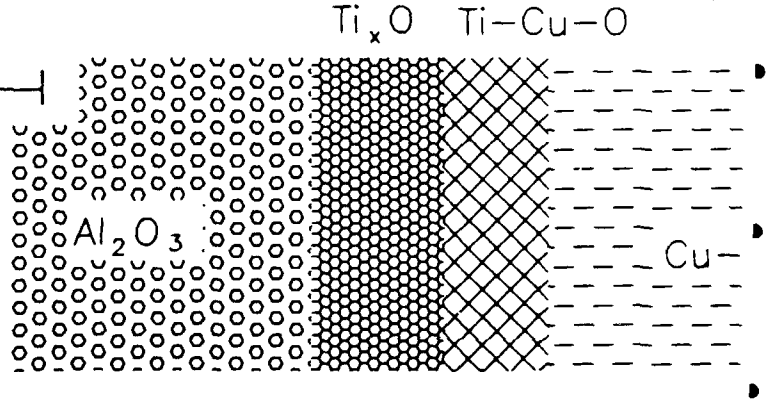

e

Figure 12 Backscattered electron image and X-ray line scans of alumina substrates immersed in Cu-5.0-w/o-Ti alloy at 1800°C for: a), c) 180-s and b), d) 300-s; e) interface morphology

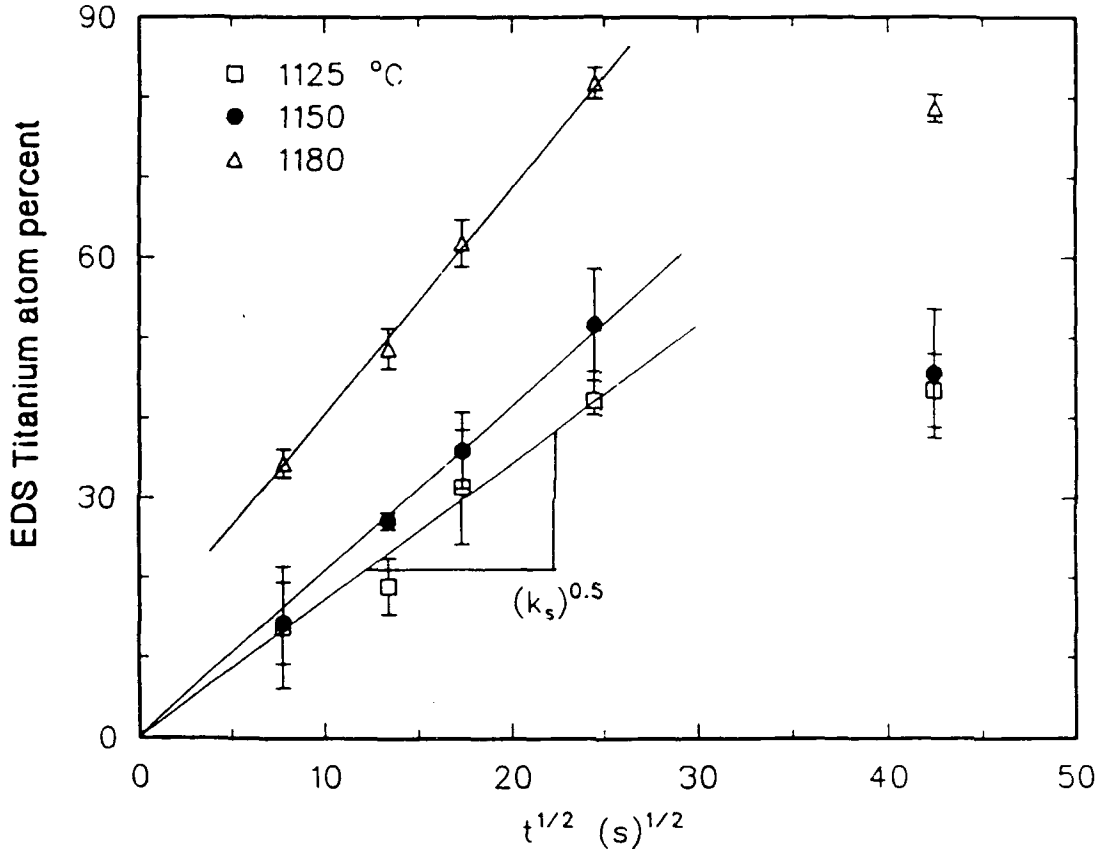

Figure 13 The rate constant k_s for the 0.5-w/o-Ti alloy

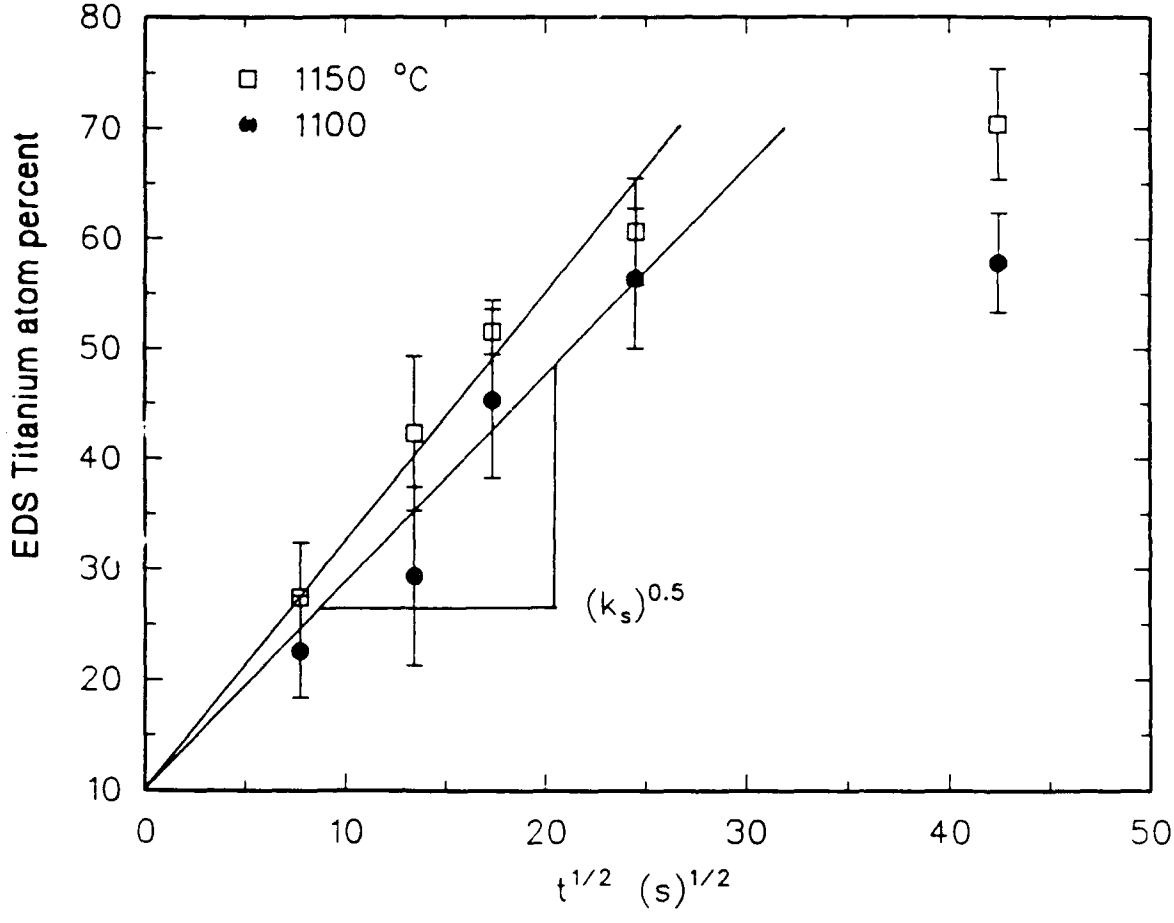

Figure 14 The rate constant k_s for the 1.0-w/o-Ti alloy

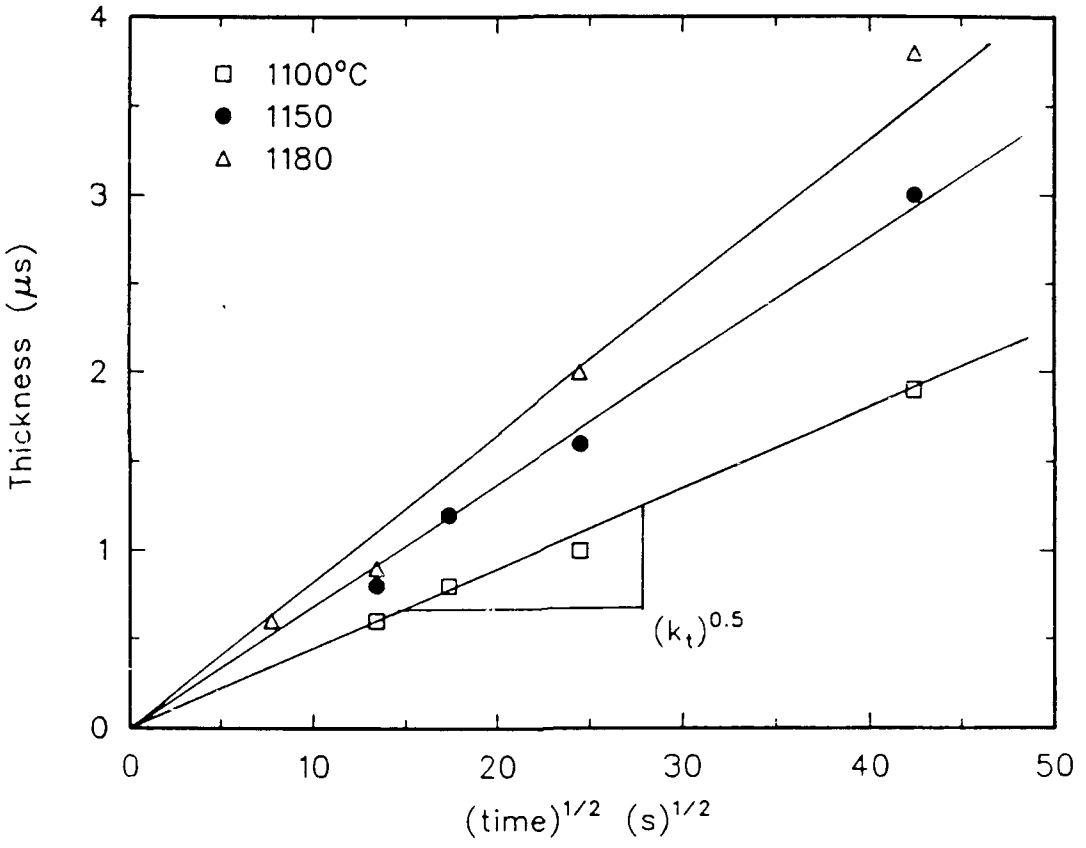

Figure 15 The rate constant kt for Cu-5.0-w/o-Ti alloys

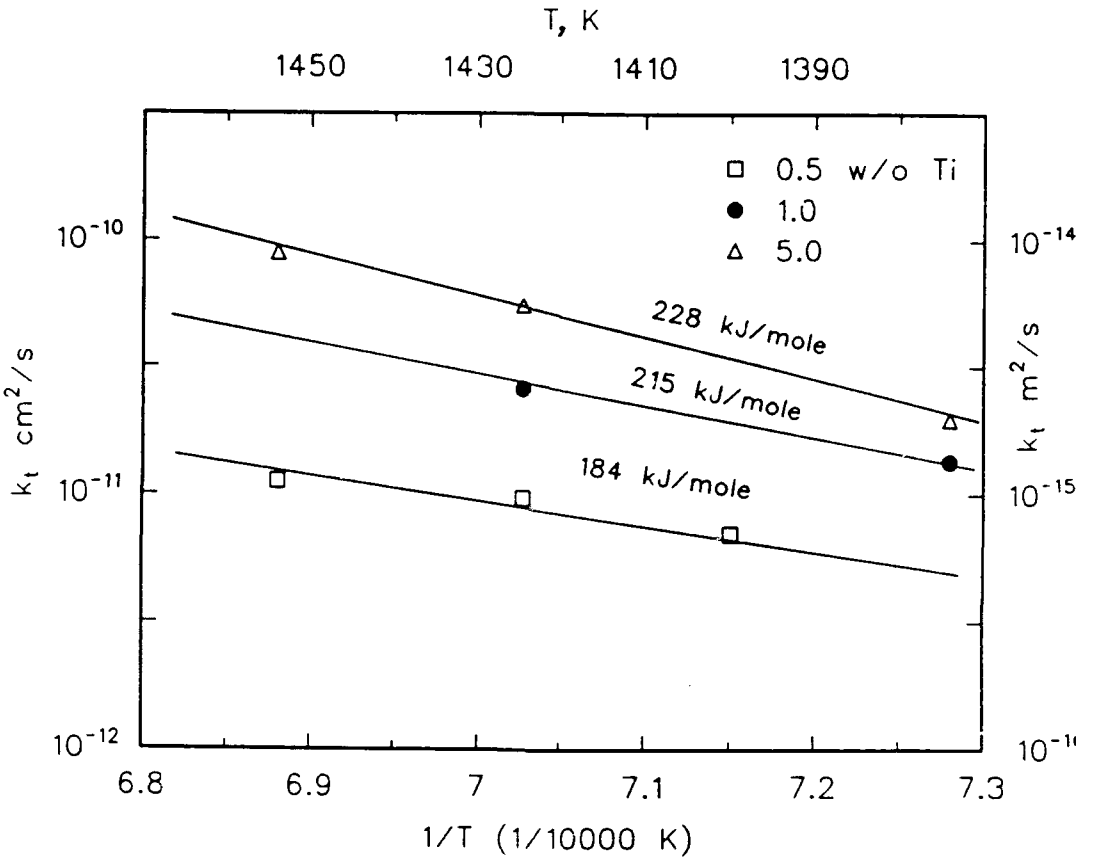

Figure 16 The activation energy of the rate controlling step in the reaction layer growth

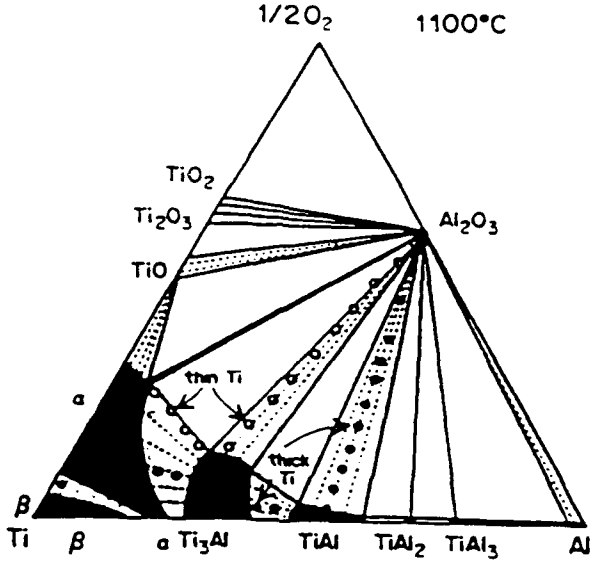

Figure 17 The Ti-Al-O ternary phase diagrams showing the virtual diffusion paths in an Al_2O_3/Ti couple [13]

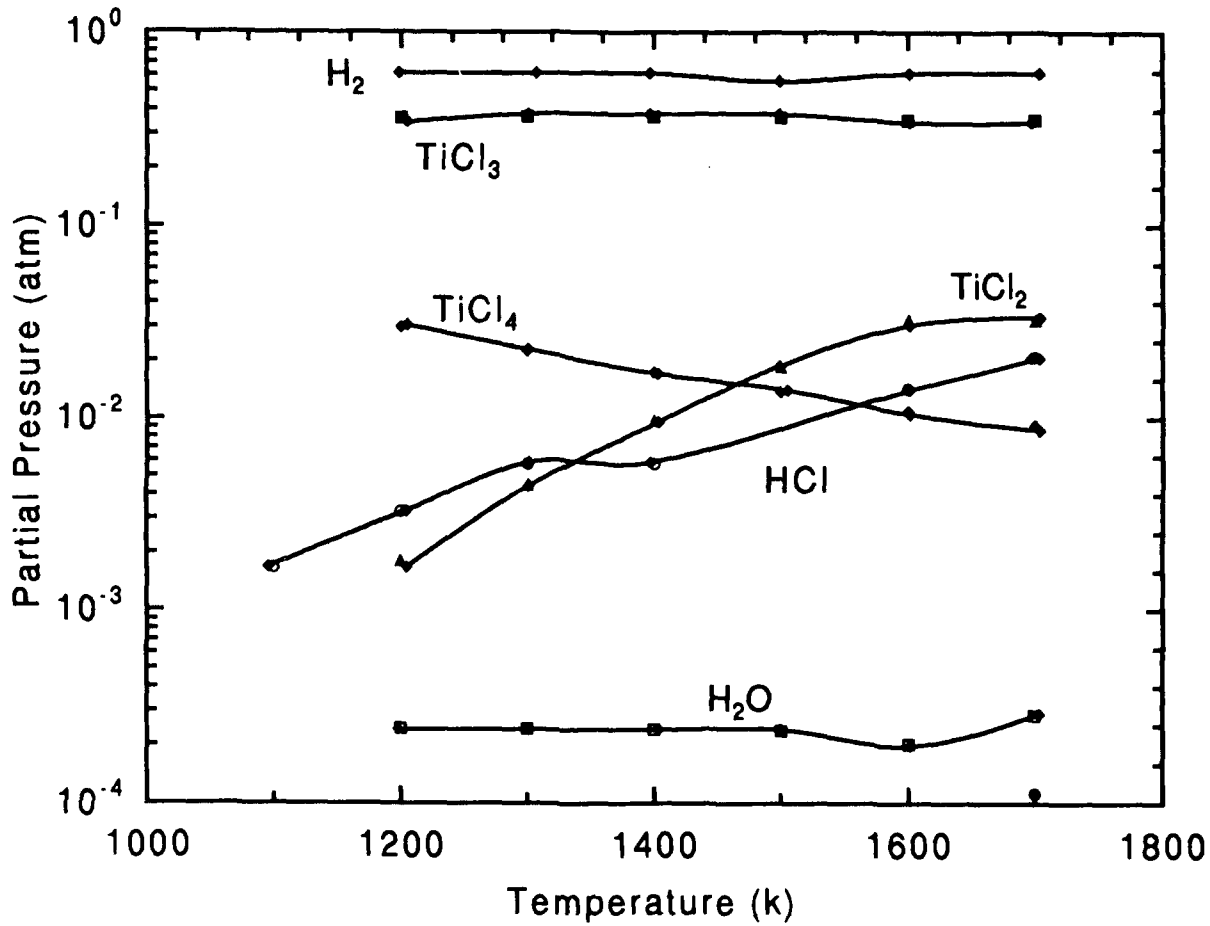

Figure 18: Equilibrium vapor pressures of various gaseous species in the HCl activated system.

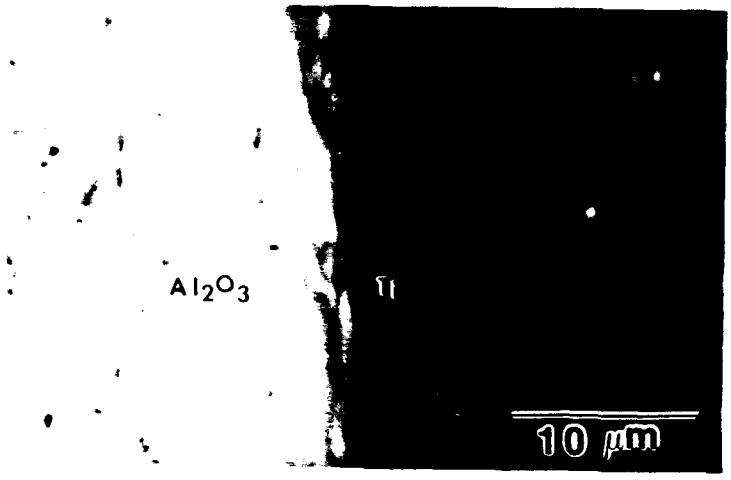

a)

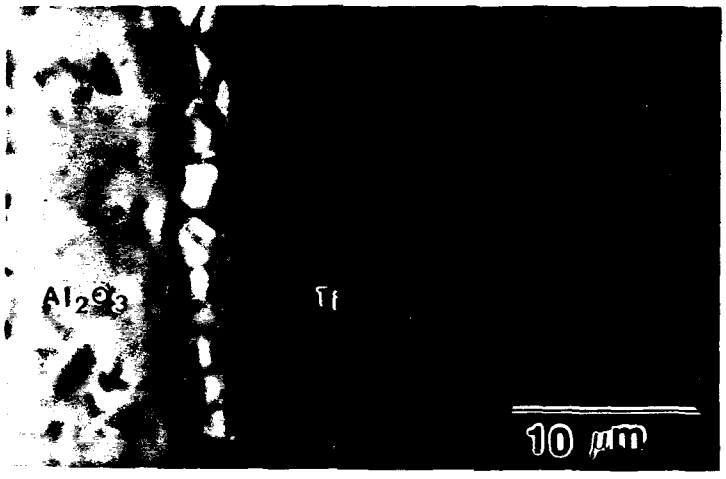

b)

Figure 19: Backscatter electron image of the interfacial region of the titanium coated Al_2O_3 substrate; a)1300K, 16.5 hours b)1150K, 13.0 hours.